Jan Verspecht bvba

Gertrudeveld 15
1840 Steenhuffel
Belgium

email: contact@janverspecht.com
web: http://www.janverspecht.com

Broad-Band Poly-Harmonic Distortion (PHD) Behavioral Models From Fast Automated Simulations and Large-Signal Vectorial Network Measurements

David E. Root, Jan Verspecht, David Sharrit, John Wood and Alex Cognata

Broad-Band Poly-Harmonic Distortion (PHD) Behavioral Models From Fast Automated Simulations and Large-Signal Vectorial Network Measurements

David E. Root, *Fellow, IEEE*, Jan Verspecht, *Senior Member, IEEE*, David Sharrit, John Wood, *Senior Member, IEEE*, and Alex Cognata

Abstract—We present an optimal experiment design methodology and a superior and fully automated model generation procedure for identifying a class of broad-band multiharmonic behavioral models in the frequency domain. The approach reduces the number of nonlinear measurements needed, minimizes the time to generate the data from simulations, reduces the time to extract the model functions from data, and when used for simulation-based models, takes maximum advantage of specialized simulation algorithms. The models have been subject to extensive validation in applications to real microwave integrated circuits. The derived model is valid for both small and large amplitude drive signals, correctly predicts even and odd harmonics through cascaded chains of functional blocks, simulates accurately load–pull behavior away from 50 Ω, and predicts adjacent channel power ratio and constellation diagrams in remarkably close agreement to the circuit model from which the behavioral model was derived. The model and excitation design templates for generating them from simulations are implemented in Agilent Technologies' Advanced Design System.

Index Terms—Design automation, frequency-domain analysis, microwave measurements, modeling, nonlinear circuits, nonlinear systems, small-signal mixer (SM) analysis.

I. INTRODUCTION

T HE DESIGN of broad-band microwave systems and modules for modern instrumentation applications presents a significant challenge. A typical microwave system will contain several active integrated-circuit (IC) components, as well as passive elements, each of which may be distributed in nature. Such a system is often too complex to permit complete simulation of the nonlinear behavior at the transistor level of description. A complete system simulation can become practical, however, provided the design is done at a higher level of abstraction, using behavioral models of the nonlinear blocks or ICs. The behavioral models must describe both the frequency-dependent nonlinear behavior of the ICs and properly describe the propaga-

tion of harmonic and intermodulation distortions through the system to enable the designer to meet rigid specifications, while being simple enough to allow rapid simulation. The resulting behavioral model must provide complete intellectual property (IP) protection; it must be fundamentally impossible to reverse engineer the underlying circuit or circuit-level model from the behavioral model. This promotes IP sharing and reuse.

Behavioral models can be formulated in the time, frequency, or mixed domains [1], [2, Ch. 3 and 5]. Time-domain behavioral models are usually formulated by the specification of a nonlinear ordinary differential equation. They are naturally best suited, therefore, to systems that can be approximated efficiently by lumped nonlinearities. Time-domain models have an advantage in that they can execute properly in all modes of simulation, including transient analysis (TA), harmonic balance (HB), and circuit envelope (CE) analysis. However, in the latter two cases, the solution algorithms must transform back and forth between the time and the respective simulation domains, at each iteration, using, for instance, the fast Fourier transform (FFT). This can increase the simulation time.

A model formulated in the mathematical language native to the simulation algorithm used to most efficiently solve the problem has the potential to be more efficient. In particular, it is natural, if less familiar, to formulate a model of a microwave circuit in the frequency domain for accurate and efficient HB simulation. Another major advantage of a frequency-domain model is that it is better suited to model dispersive distributed components over a wide bandwidth, as are common in RF, microwave, and millimeter-wave systems. Moreover, the structure of the model considered here is amenable to direct identification, in the frequency domain, from simple frequency-domain excitations using a vector nonlinear network analyzer (VNNA). In contrast, the approach of [3] requires conversion of the frequency-domain excitations and system responses to the time domain for the purpose of model identification and implementation.

The infrastructure and process of behavioral modeling involves at least three interrelated components. The first is the model (or model class) itself. This means, for example, the specification of the order and structure of the differential equation in the time domain, or the number of harmonics and the structure of the input-to-output spectral mapping in the frequency domain. The second component of behavioral modeling is the excitation

design. This refers to the set of experiments (stimuli) required to elicit the system response sufficiently to identify the model parameters. The third is the model generation procedure. This is the algorithm used to determine the model parameters from the data obtained from the experiments.

Requirements for a robust behavioral modeling process include the ability to characterize, quickly, the component or circuit-level model, and construct the behavioral model in a repeatable, procedural, and automated way. The excitations should be as few in number as possible for the particular model class. Ideally, each experiment can be used to identify a particular model parameter uniquely and independently. In an optimal design, each additional experiment provides totally new, or "orthogonal" information [4].

In [5], a black-box frequency-domain behavioral model, generalized from the work of [6], was identified from real automated measurements on a wide-band microwave IC amplifier using a VNNA [7]. This measurement-based behavioral model was experimentally demonstrated to be valid for small and large amplitude drive signals, correctly predict even and odd harmonics, and simulate accurately even into impedances different from the 50-Ω environment in which the data was measured. One limitation of the usefulness of the model is the limited dynamic range of the VNNA instrument, which can be estimated from the data in [5]. Nevertheless, the results of [5] demonstrate that the behavioral model, together with the automated VNNA measurements to identify it, provide a general, practical, and useful tool. Moreover, recent large-signal hardware developments [8] significantly demonstrate improved dynamic range that will only increase the general utility of the approach. Another limitation of [5] is the suboptimal nature of the experiment design and model identification algorithm. That is the subject of this study.

In this paper, we present a superior experiment design approach and an improved algorithm for identifying, from this different set of data, the behavioral model discussed in [5]. In fact, the approach is both orthogonal and optimal in the sense it uses the minimum number of independent measurements. We apply the new approaches to generate accurate behavioral models from detailed circuit-level models of real microwave ICs using the nonlinear simulator as a virtual instrument. New results, including the prediction of ACPR and *I–Q* constellation diagrams by the behavioral model are presented and validated. In combination with [5], this study completes the "closing of the loop" to include both simulation- and measurement-based approaches to generating the same frequency-domain nonlinear behavioral model.

In Section II, we briefly review the poly-harmonic distortion (PHD) behavioral model. In Section III, we describe the new experiment design and model generation algorithms. In Section IV, we compare the approach to other work in the literature. In Section V, we present new results validating the PHD model against the circuit model from which it was derived.

II. PHD Model Formulation

The target behavioral model for this study was presented in [5], which generalized the work first presented in [6] and sum-

marized in [2, Ch. 5]. It is a "black-box" behavioral model requiring no *a priori* knowledge of the device physics or circuit configuration of the nonlinear component. The model theory derives from a multiharmonic linearization around a periodic steady state determined by a large-amplitude single input tone. For this reason, we refer to the model as the PHD model. The assumption is that the system to be modeled can depend in a strongly nonlinear way on its large-signal drive, but nevertheless responds linearly to additional signal components at the harmonic frequencies considered as "small" perturbations around the time-varying system state. This is referred to as the "harmonic superposition" principle [6]. The harmonic superposition principle has been shown in [2, Ch. 5], [5], and [6] to be an approximation well satisfied by power amplifiers of several different classes and for applications where the functional block is inserted into impedance environments mismatched somewhat from 50 Ω at both the fundamental and harmonics. In real applications, for example, these harmonic terms can result from nonlinearities created from previous amplification stages or reflections from nonlinear devices at the next input stage of a multistage amplifier. The broad-band nature of the model is essential for modeling the frequency dependences of the nonlinear responses of such microwave ICs as multiple-octave traveling-wave amplifiers and other components useful in instrument applications.

The model is defined by (1) and (2) in the frequency domain relating complex transmitted and scattered waves at each port p and harmonic index k to a linear combination of terms in the incident waves *and their complex conjugates* independently at each port at each harmonic. The fact that the complex conjugate terms appear is a necessary consequence of the nonanalyticity of the Jacobian, which represents the linearization around the time-varying operating point established by the single large-amplitude tone in the absence of perturbation. An alternative explanation follows from the mixer analysis of Section III. The sums in (1) are over all port indexes q, and harmonic indices l (DC is excluded in the cases presented here so the sum over l starts at the fundamental. In general, this method can easily be extended to include the dc term, in which case, the sum starts from index 0.)

$$B_{pk}(|A_{11}|, f) = \sum_q \sum_{l=1,\ldots,M} S_{pq,kl}(|A_{11}|, f) \cdot P^{k-l} \cdot A_{ql}$$
$$+ \sum_q \sum_{l=1,\ldots,M} T_{pq,kl}(|A_{11}|, f) \cdot P^{k+l} \cdot A_{ql}^*$$

$$\text{(1)}$$

$$T_{p1,k1} = 0. \tag{2}$$

In (1), $P = \exp(jArg(A_{11}))$ is a pure phase that, along with the magnitude-only dependence on A_{11} of the S and T functions, is a necessary consequence of the assumed time invariance of the underlying system. A redundancy, introduced by summing over the fundamental components ($l = 1$) in addition to the harmonics in (1), requires the imposition of the additional constraints given by (2). For all but one of the applications demonstrated in Section VI, we consider a two-port amplifier model with five harmonics. The final result was obtained considering only three harmonics.

III. EXCITATION DESIGN

In [5], the excitation design for the PHD model was based on perturbing the nonlinear component under a large-signal drive by applying several small tones one at a time at each port and at each harmonic of the fundamental. This was done for each harmonic up to the maximum number needed for the model (or, for the measurement-based case, the limitation of the instrument's bandwidth). The structure of model (1) and (2) is such that, in principle, the S and T coefficients at each harmonic can be extracted directly from three measurements. These measurements are: 1) the responses at each port and at each harmonic frequency to the large tone without perturbation; 2) the responses to the simultaneous excitation of the large tone and a small-signal perturbation tone; and 3) the responses to a simultaneous excitation of the large tone and a small-signal perturbation tone at a the same frequency, but different phase compared to the small tone of 2). The component of the B-wave at each port and at each harmonic has contributions from both A and A^*; the two relative phases per frequency per port for the small tones were proposed in order to provide two independent data for B from which to determine the two model coefficients (S and T) for a given harmonic frequency component of the response.

The improved experiment design is based on considering model (1) and (2) as the limiting case of a more general time-varying nonlinear system perturbed by an arbitrary small tone. Here the restriction that the frequency of the perturbation tone is exactly at a harmonic of the fundamental is relaxed. Such a system can be analyzed as a mixer. Moreover, if the perturbing tone is sufficiently small, the analysis can be considered to be that of a "small-signal mixer" (SM).

The derivation is outlined for a single port. The extension to multiple ports is obvious. We start in the time domain by representing the output wave $b(t)$ as a nonlinear function of the input wave $a(t)$ according to (3) as follows:

$$b(t) = b(a(t)). \tag{3}$$

These are real signals and, in (3), the nonlinearity is algebraic (this restriction is not necessary, but facilitates a simpler way to the result). We now consider the input signal class to be the sum of a single large tone $a_0(t)$ at frequency f_0 and a small-signal $\Delta a(t)$ at frequency f_1 as follows:

$$b(t) = b(a_0(t) + \Delta a(t)). \tag{4}$$

We assume the perturbation is small, and expand (4) in a Taylor series and keep terms only up through first order as follows:

$$b(t) \approx b_0(t) + \Delta b(t) = b(a_0(t)) + \frac{\partial b(a_0(t))}{\partial a} \cdot \Delta a(t). \tag{5}$$

Identifying $b_0(t) = b(a_0(t))$, the linear response is given by (6) as follows:

$$\Delta b(t) = \frac{\partial b(a_0(t))}{\partial a} \cdot \Delta a(t). \tag{6}$$

Since $a_0(t)$ is periodic, we can expand the first term on the right-hand side of the equal sign of (6), the conductance nonlinearity, in a Fourier series in $\omega_0 = 2\pi f_0$ as follows:

$$\frac{\partial b(a_0(t))}{\partial a} = \Lambda_{\mathrm{DC}} + \sum_{n=1}^{\infty} \left(\Lambda_n e^{jn\omega_0 t} + \Lambda_n^* e^{-jn\omega_0 t} \right). \tag{7}$$

The perturbation tone is represented in the frequency domain as follows:

$$\Delta a(t) = \delta e^{j\Omega t} + \delta^* e^{-j\Omega t}. \tag{8}$$

Here, $\Omega = 2\pi f_1$ and δ is a small (in magnitude) complex number.

Note that we are dealing with two periodic signals with unrelated fundamental periods (7) corresponding to the system response to a large tone at f_0, and (8), the small tone at f_1. Multiplying out the factors in (6) using (7) and (8) results in the following expression for $\Delta b(t)$:

$$\begin{aligned} \Delta b(t) = {} & \Lambda_{\mathrm{DC}} \delta e^{j\Omega t} + \Lambda_{\mathrm{DC}} \delta^* e^{-j\Omega t} \\ & + \sum_{n=1}^{\infty} \Big(\Lambda_n \delta e^{j(\Omega + n\omega_0)t} + \Lambda_n^* \delta e^{j(\Omega - n\omega_0)t} \\ & \qquad + \Lambda_n \delta^* e^{j(n\omega_0 - \Omega)t} + \Lambda_n^* \delta^* e^{-j(n\omega_0 + \Omega)t} \Big). \end{aligned} \tag{9}$$

For future reference, we designate the third through sixth terms of (9) as (a)–(d), respectively.

We now consider the special case where the frequency of the small tone is nearly a harmonic (integer multiple) of the fundamental of the large tone, i.e., $\Omega = m\omega_0 + \varepsilon$. Here, ε is a positive infinitesimal. The frequency offset will allow us to refer to the stimulus at frequency Ω as the *upper sideband stimulus* at frequency $m\omega_0$.

The objective is to pick out the complex spectral components of the response $\Delta b(t)$ in the frequency domain at the harmonic frequencies $l\omega_0$ for nonnegative integers l $(l = 1, 2, 3, \ldots)$. We can break up the contributions into terms proportional to δ and δ^* separately. For simplicity, we assume there are no dc components in the following. Looking at terms (a) and (b) in (9), we find that the contributions that are proportional to δ are A_{l-m} for $l - m \geq 1$ or A_{m-l} for $l - m \leq -1$. From terms (c) and (d) in (9), we obtain the terms proportional to δ^*. The results are A_{l+m} for $l + m \geq 1$ and $A_{-(l+m)}$ for $l + m \leq -1$.

Thus, we can write the linearized response Δb_{lm} at the lth harmonic in response to the perturbation at the mth harmonic as

$$\Delta b_{lm} = S_{lm} \delta + T_{lm} \delta^* \tag{10}$$

with the coefficients given in terms of the harmonic series for the conductance as described above. This allows the behavior of the S and T coefficient functions to be related to the Volterra representation of the original nonlinearity.

If we compare (10) (note we omitted the port indexes here) to (1), we can see that the coefficients of the PHD model can be explicitly calculated in terms of the Fourier series of the system conductance nonlinearity of (7) in the limit as ε goes to zero.

TABLE I
OUTPUT OF SM SIMULATION $F_0 = 3$ GHz, $M = 2$, AND ORDER $= 8$

Spectral Comp. Freq (GHz)	N	M	Sideband Designation	Model Coefficients
$0 + \varepsilon$	-2	1	Upper	$S_{i0,j2}$
$3 - \varepsilon$	3	-1	Lower	$T_{i1,j2}$
$3 + \varepsilon$	-1	1	Upper	$S_{i1,j2}$
$6 - \varepsilon$	4	-1	Lower	$T_{i2,j2}$
$6 + \varepsilon$	0	1	Upper	$S_{i2,j2}$
$9 - \varepsilon$	5	-1	Lower	$T_{i3,j2}$
$9 + \varepsilon$	1	1	Upper	$S_{i3,j2}$
$12 - \varepsilon$	6	-1	Lower	$T_{i4,j2}$
$12 + \varepsilon$	2	1	Upper	$S_{i4,j2}$
$15 - \varepsilon$	7	-1	Lower	$T_{i5,j2}$
$15 + \varepsilon$	3	1	Upper	$S_{i5,j2}$
$18 - \varepsilon$	8	-1	Lower	$T_{i6,j2}$
$18 + \varepsilon$	4	1	Upper	$S_{i6,j2}$
$21 + \varepsilon$	5	1	Upper	
$24 + \varepsilon$	6	1	Upper	
$27 + \varepsilon$	7	1	Upper	
$30 + \varepsilon$	8	1	Upper	

Keeping track of the ε term, we can also see that the S coefficients are the responses at the *upper sideband* and that the T coefficients, with the same indices, are the *lower sideband* responses. This is the direct way to identify the PHD model from this SM analysis.

From basic mixer theory, if a signal consisting of the sum of two tones at (angular) frequencies ω_0 and Ω, respectively, are put through a nonlinear device, the discrete frequencies of the response fall at frequencies ω_{mix} satisfying

$$\omega_{\mathrm{mix}} = \pm N\omega_0 \pm M\Omega \qquad (11)$$

for N and M provided $\omega_{\mathrm{mix}} \geq 0$ (to keep from double counting). The integers N and M correspond to the order of the mixing terms. If we further assume that one tone is always small compared to the other, we can simplify (11) by assuming all terms beyond the first order of the small tone can be neglected. This is equivalent to restricting $M = \pm 1$.

We now set $\Omega = m\omega_0 + \varepsilon$. For $\varepsilon = 0$, we get the degenerate case of the harmonically related experiment of the design approach of [5]. This corresponds to a small tone at the mth harmonic of the fundamental. Considering ε as a positive infinitesimal allows us to keep separate track of the two different terms that contribute to the same frequencies in the output spectrum due to different origins.

We consider the example for which $\omega_0 = 3$ GHz, $m = 2$ (small tone at 6 GHz), and order $= 8$. Here "order" is the order of the HB analysis part of the SM analysis used. The spectral response, linear in the perturbation signal, can, therefore, be represented as in Table I. This represents the difference between the full output spectrum of the system with one large

and one small tone, and the output of the system with only the single large tone (no small tone added). The second column is the order of the large tone contributing to the frequency component specified in that row. A negative sign means the negative frequency component. The third column indicates the order of the small tone (recall only terms for $M = \pm 1$ are considered). The fourth column indicates whether the contribution to this frequency is at the lower or upper sideband (by keeping track of ε). We could also distinguish the sidebands simply by checking the value of M. There is only one contribution at frequency $= 0$; this is an upper sideband. There are two contributions to the next group of frequencies, from 3 to 18 GHz, in the same alternating order of lower and upper sidebands. This follows from the two different contributions of orders of the large and small tones that can combine to give terms at each of these frequencies. For example, at 9 GHz, the fifth-order contribution from the large tone at 3 GHz combines with the negative frequency component of the small tone at 6 GHz to give a tone at $5 * 3$ GHz $+ 2 * 3$ GHz $* (-1) = 9$ GHz. The upper sideband comes from a combination of a first-order term in the large tone with the positive term from the small tone because $1 * 3$ GHz $+ 1 * 2 * 3$ GHz $= 9$ GHz. There are no other combinations possible to end up at 9 GHz. Eventually, at 21 GHz, there are only upper sidebands. This is because for a lower sideband to exist, it must correspond to the solution of (12) as follows:

$$21 \text{ GHz} = n \cdot 3 \text{ GHz} - 2 \cdot 3 \text{ GHz}. \qquad (12)$$

The solution to (12) is $n = 9$, which is beyond the order $= 8$ value, and thus it is not calculated. This condition persists for the rest of the frequencies. There is a table like this for each value of m.

In a simulation, using SM analysis, to be described, we can set $\varepsilon = 0$. In a real measurement, however, ε must be kept small, but nonzero, typically approximately 1 kHz. In this case, there are always both upper and lower sidebands at each frequency provided their magnitude is large enough to measure and if the frequency offset ε is not too small to resolve the two sidebands. Therefore, in a real measurement, there would be second rows in the table just below 21, 24, 27, and 30 GHz (for this example) corresponding to the lower sidebands.

Through these calculations we determine the S coefficients from the upper sideband responses and the T coefficients from the lower sideband responses. This demonstrates that we only need a *single* upper sideband (small) signal excitation at each port at each harmonic from which to extract both S and T coefficients corresponding to upper and lower sidebands, respectively. We do not need (at least) two small tones of different relative phases as required by the method of [5].

For the simulation-based approach, the Agilent Advanced Design System (ADS) SM analysis is used as the excitation. A key advantage of this excitation is that the simulation is much faster than a two-tone HB analysis since the only HB analysis done in the former is that for the single large tone. The linearization of the system is done automatically using the Jacobian information already computed by the simulator for the one-tone HB analysis. Another advantage is that the SM analysis results in exactly (to numerical precision) the

linearized response of the system under a large-signal drive to the perturbations at the harmonics. A two-tone HB analysis, even for one of the tones being small, would produce additional mixing terms, which increases the size of the dataset and requires a more complicated regression analysis to identify the model.

The simulation is specified by stepping the small-signal offset frequency from zero to some upper multiple of the fundamental large tone at each port separately. For each of these conditions, an SM analysis is performed for each power level and fundamental frequency over which the model is to be used. The result of the analysis is precisely (for each fundamental) the set of data shown in Table I. A nonzero offset, corresponding to ε in the range 1 Hz–1 kHz, is used to get the ordering as shown in Table I. The results for any values of ε in this range are usually identical to five significant digits. For $\varepsilon = 0$, the order of the rows of Table I may differ.

The model identification (generation) algorithm directly extracts the S and T coefficients at each power level for each fundamental frequency. The values of S and T at each power and frequency, for all combinations of indices, are written to the final model *Citifile*.

IV. MODEL IMPLEMENTATION

The PHD model is implemented in the Agilent ADS simulator as a sub-circuit using the frequency-domain device (FDD) built-in component. The measured and identified S and T model functions are stored in a two-dimensional *Citifile* format. The dimensions correspond to the amplitude and fundamental frequency of the large-signal input tone, respectively. Equations (1) and (2) appear in a text file read by the model. A data-access component (DAC) links the tabulated data to the model and performs multidimensional interpolation during the simulation.

V. DISCUSSION

The work of [5] resulted in very accurate measurement-based behavioral models with a well-defined and procedural experiment design and model identification procedure. However, that experiment design required many more measurements than necessary. That method requires, in practice, injecting small tones at several different phases relative to the large input tone (at each port and at each harmonic). The need for several phases arises from two independent reasons. Fundamentally, starting from (1), injecting small tones at precisely harmonics of the fundamental requires tones at a minimum of two phases since the contributions from the separate mechanisms described by the new approach overlap in frequency (the upper and lower sidebands coincide) and cannot be separated. Beyond this, since the hardware cannot specify the phase of the small tones (it can measure them, but not specify them), a number of measurements (at random phases) are needed to ensure a well-conditioned solution to the regression equations. This last requirement multiplies the number of needed measurements by an additional factor typically from 2 to 6.

In contrast, the new mixer-based offset tone method presented in this paper enables experiments in which small tones of only a single—but arbitrary—phase for frequencies near

the harmonics are sufficient to identify the model coefficients. This is because with actual frequency offsets relative to the harmonics, the responses of the system occur at different nonoverlapping frequencies (the sidebands are distinct) and measurable independently. It is important to emphasize that both the amplitude and phase of each of the two ε-offset sidebands must be measured in order to identify the model of (1). This cannot be done with most available measurement systems, hence, the requirement of an advanced system with the capabilities of a VNNA. The ε-offset measurements can be done using the narrow-band modulation mode of the VNNA.

The new experiment design presented here dramatically reduces the number of required measurements for both measurement- and simulation-based applications. It, therefore, reduces the data acquisition time and reduces both the size and complexity of the data file. In the case of the simulation-based application, the new experiment design, based on the SM analysis, results in the exact linearization of the system around the large-tone already calculated by the simulator as part of the HB solution corresponding to one-tone excitation. The linear response is produced by a direct evaluation using the Jacobian information from the single-tone HB analysis. The SM analysis is much more efficient than using a two-tone (one large tone and one small tone) HB simulation. The SM analysis ensures the virtual data is uncorrupted by harmonics of the smaller tones that would result from a direct application of the experiment design of [5]. The new experiment design also significantly reduces the computer memory requirements and complexity of the resulting data. The new identification procedure results in a dramatic simplification of the model generation process. The S and T functions are extracted directly and independently from a single SM experiment design. Each independent experiment yields a different set of S and T functions, therefore, resulting in the optimal procedure for this model class, demonstrating the "orthogonality" principle.

Beyond this, the new methods of excitation design and model identification correspond to a more general representation of nonlinear systems than the amplifier-specific form (1) of the PHD nonlinear behavioral model. The general approach embodies a scalable representation of multiport broad-band linear time-varying systems. The PHD model emerges as a special case for a system stimulated by signals of the class considered here. The general case obviously includes linear mixers. The extension to mixers with distortion will be presented elsewhere.

References [2, Ch. 3] and [9] present experiment designs somewhat similar to this study in that they are based on applying a small tone offset from a large tone to obtain responses at three different frequencies (per offset) from which a behavioral model can be identified. However, neither of these studies explicitly take into account the harmonics generated by the nonlinear device. Moreover, the models identified in [2, Ch. 3], [9], and [10] are not identical to model (1) used in this study. Therefore, the model identification algorithm is different as well.

Reference [11] presents an experiment design similar to that of [2, Ch. 3] and [9]. However, [11] deals with a simplified version of the model of (1), neglecting all harmonics and the frequency dependence of the large tone. Moreover, [11] does

not discuss the use of the specialized SM simulation algorithm, which applies without the need for a nonzero offset frequency, in order to most efficiently generate data from simulations of detailed circuit models.

Reference [12] presents an extraction of the conversion matrix of a nonlinear two-port from VNNA measurements using a methodology very similar to the experiment design presented in this study. However, [12] does not relate the experiment design to a nonlinear model, such as (1), implemented in the simulator that can be used for broad-band designs over a continuous range of signals. Moreover, the three aspects (model, experiment design, and model identification) presented in this study are formulated directly in terms of incident, transmitted, and reflected (pseudo) waves. This represents a more direct link with the measurements, as well as S-parameter theory, without the need for transformations to and from the admittance representation. Further connection between this study and conversion matrices can be found in [13].

VI. RESULTS

The experiment design and model generation procedure described here were applied to a detailed circuit-level model of a wide-band microwave IC amplifier, the Agilent Technologies' HMMC-5200 [14], the same component that was used for the experimental work in [5]. This is a dc–20-GHz 10-dB amplifier with internal feedback designed for use as a cascadable gain block in a variety of microwave circuit applications. It contains eight GaAs HBTs of two different sizes, configured as a compound modified Darlington feedback pair, operating in class A.

The circuit model is placed in a simulation template in ADS. The template applies a single-tone excitation in HB analysis to the input of the amplifier model terminated with 50 Ω. The amplitude and frequency of the tone are swept over the anticipated useful range of the resulting behavioral model. The template also allows variation of other circuit parameters such as biases on dc pins that may be distinct from the RF ports. At each of these conditions, the template invokes ADS SM analysis to provide the derivative information with respect to the large-signal HB solution. The simulated results are exported from the ADS dataset to a processing script. The new identification algorithm is used to directly solve for the S and T coefficients of the PHD model as functions of power, frequency, and the parametric variables such as supply voltage. The PHD model functions are tabulated and stored in a multidimensional *Citifile*. The FDD implementation of the PHD model reads the *Citifile* and dynamically interpolates during simulation.

The first six figures show the comparison of the PHD behavioral model, generated using the current approach, compared to the underlying circuit model from which it was derived. Fig. 1 shows the comparison for amplifier gain (in decibels) as a function of incident power (in dBm) over a decade range of frequency (from 600 MHz to 6 GHz) from highly linear operation to over 2.5 dB compressed. Fig. 2 compares the AM–PM characteristics of the circuit-level model and the derived PHD behavioral model over the same range of operating conditions. Figs. 3 and 4 show the comparison for the reflection amplitude
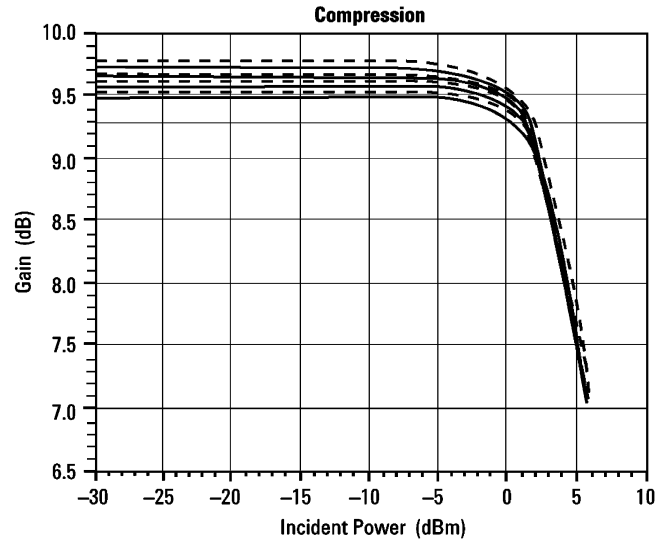

Fig. 1. Simulation-based PHD model (solid lines) compared to underlying circuit-level model (dashed lines) from which it was derived. Gain in decibels versus input power in dBm at different fundamental frequencies. The frequency range is from 0.6 to 6 GHz.
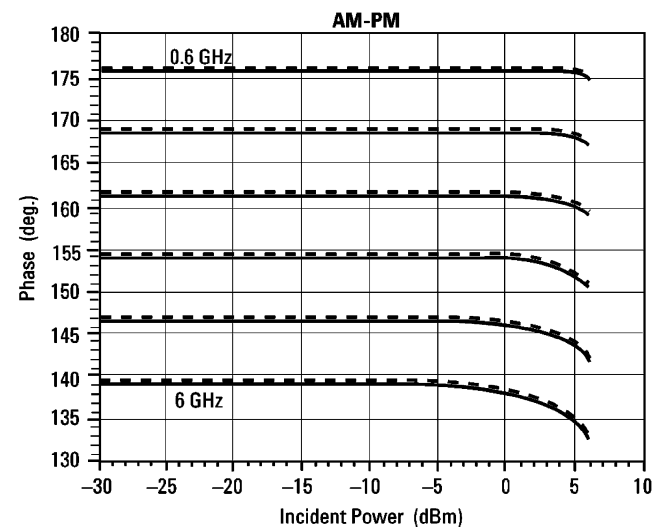

Fig. 2. Simulation-based PHD model (solid lines), compared to underlying circuit-level model (dashed lines) from which it was derived. AM–PM in degrees versus input power in dBm at different frequencies.

and phase. In all cases, over the full range of compression and full range of frequencies, the PHD behavioral model is an excellent representation of the circuit model's behavior.

Fig. 5 compares the circuit-level and PHD behavioral models in spectral regrowth envelope simulations using an RF carrier modulated by a North American Digital Cellular (NADC) signal as stimulus. The agreement is quantified in Table II in terms of upper and lower channel ACPR and main channel power. The agreement is excellent. Fig. 6 shows the corresponding constellation diagrams from the circuit-level model and the PHD model. The agreement is excellent. It should be remarked that the real IC may exhibit certain nonlinear effects (e.g., subharmonic generation) that might not be described by the circuit model and are, therefore, not included in the subsequently derived PHD behavioral model. The ultimate test of the utility
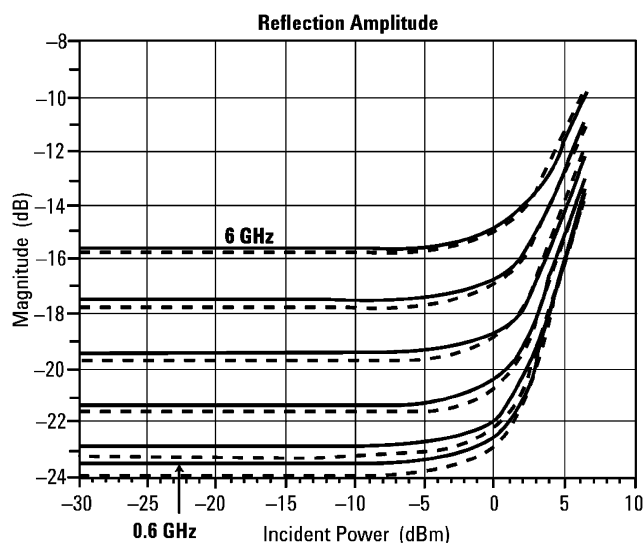
Fig. 3. Simulation-based PHD model (solid lines), compared to underlying circuit-level model (dashed lines) from which it was derived. Reflection match in decibels versus input power in dBm at different frequencies.
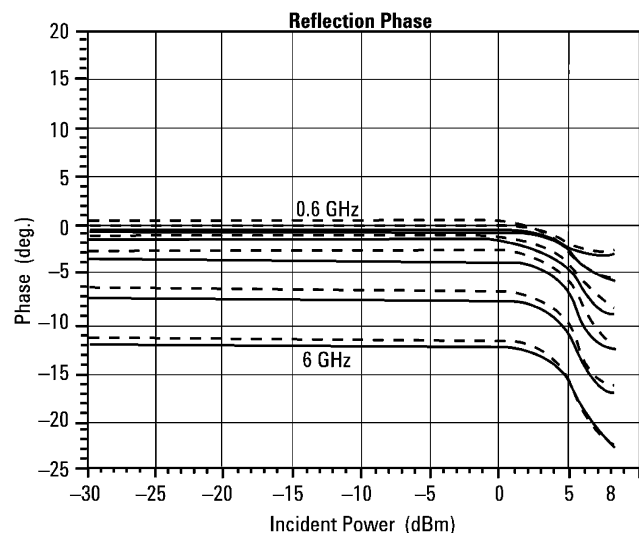

Fig. 4. Simulation-based PHD model (solid lines), compared to underlying circuit-level model (dashed lines) from which it was derived. Reflection phase in degrees versus input power in dBm.
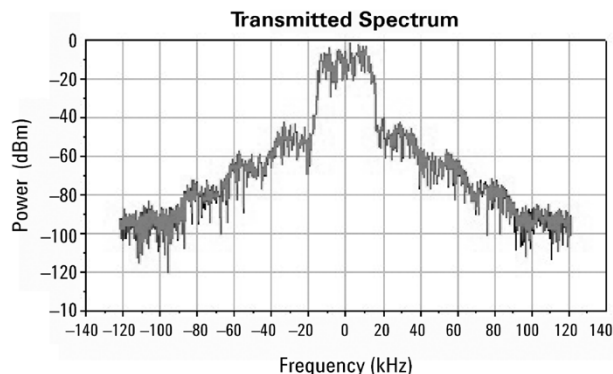

Fig. 5. Simulation-based PHD model (gray) compared to underlying circuit-level model (black) from which it was derived. Transmitted spectrum versus frequency offset. The agreement is so good it is difficult to distinguish the black under the gray.

TABLE II
MAIN AND ADJACENT CHANNEL POWER

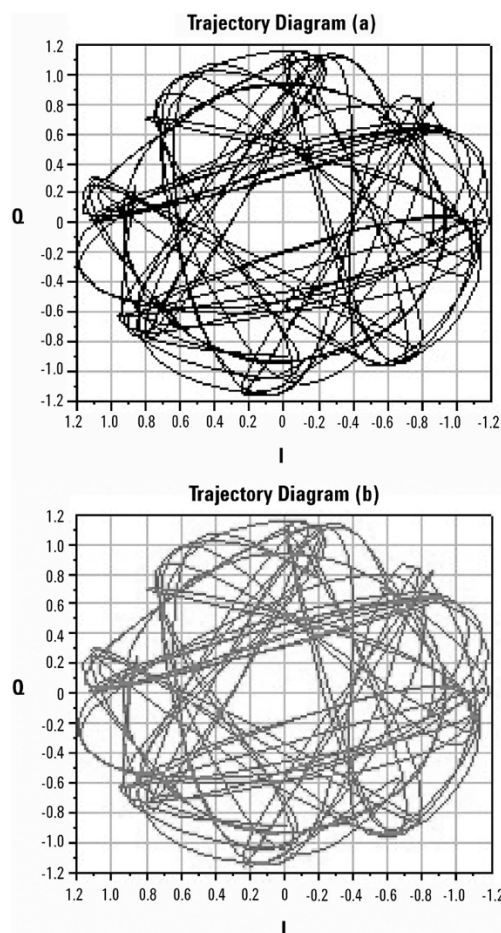|	Lower Channel ACPR	Upper Channel ACPR	Main Channel Power (dBm)
IC Circuit-Level Model	-18.572	-18.991	9.276
PHD Behavioral Model	-18.578	-18.985	9.256

Fig. 6. Simulated trajectory diagrams. (a) Circuit-level model (black). (b) Simulation-based PHD model (gray) derived from the circuit model.

Fig. 7, reproduced from [5], shows the experimental setup using the VNNA with two sources and a switch to implement the introduction of the small tones to each port. In contrast with the original experiment design of [5], the narrow-band modulation mode of the VNNA is required to make the measurements with the narrowly offset tones characteristic of the improved method described in this study.

Figs. 8 and 9 show results comparing circuit-level and PHD behavioral models in cascade. The cascade includes ideal attenuators between each amplifier to ensure that the amplifiers are not overdriven, and yet the actual input and output impedances are presented to the preceding and successive stages in the cascade. In this validation exercise, the PHD model includes three harmonics. Fig. 8 shows the amplitude of the second harmonic at the output of the second amplifier (in decibels) as a function of incident power over a decade of bandwidth. Fig. 9 shows the

of the PHD model for amplifiers under complex modulated signals requires experimental characterization of the IC under these conditions, which has yet to be done.
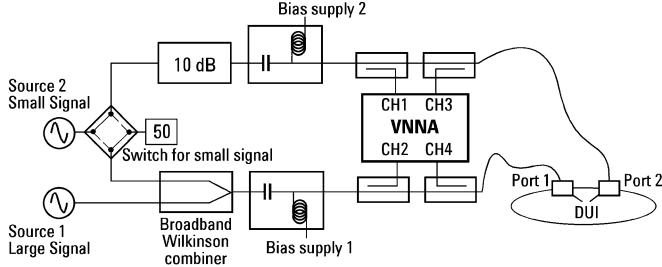
Fig. 7. Schematic connection of the VNNA for the large- and small-signal perturbations to the device-under-test (DUT). The hardware configuration is identical to that of [5]. Unlike the method of [5], the current approach can be implemented with small tones (source 2) injected at frequencies *slightly offset in frequency* from harmonics of the fundamental tone (source 1). The results are measured in the narrow-band modulation mode of the VNNA.
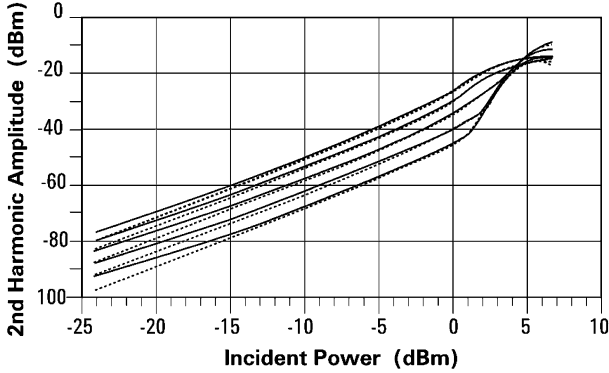

Fig. 8. Two amplifier models in cascade, circuit-level models (dashed lines), and derived PHD behavioral model (solid lines). Second harmonic power (in dBm) at the output of the second amplifier as a function of the incident power (in dBm). Frequencies range from 0.6 to 6 GHz.
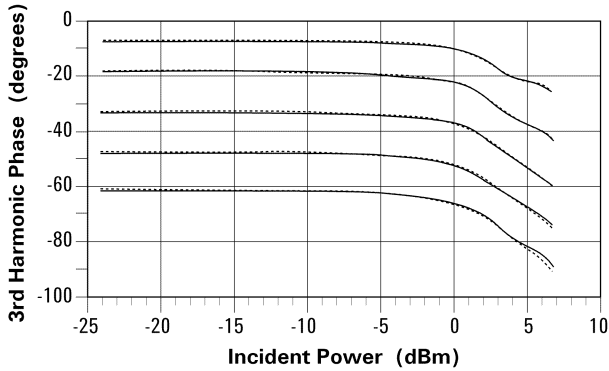

Fig. 9. Two amplifier models in cascade, circuit-level models (dashed lines), and derived PHD behavioral model (solid lines). Third harmonic phase (in degrees) at the output of the second amplifier as a function of the incident power (in dBm). Frequencies range from 0.6 to 6 GHz.

phase of the third harmonic at the output of the second amplifier. In both cases, the agreement is excellent. Moreover, we have validated the comparison for a string of ten cascaded amplifiers (not shown) with similar results. This validates the claim that the PHD model can predict well the propagation of vector distortion through chains of nonlinear components.

VII. CONCLUSIONS

We have presented an improved experiment design and improved model generation procedure for the broad-band PHD nonlinear behavioral model in the frequency domain. The model

has been validated for a wide-band microwave amplifier IC. The model, implemented in Agilent ADS, is very accurate for a wide variety of nonlinear figures-of-merit, including AM–AM, AM–PM, harmonics, load–pull, and time-domain waveforms, even when used beyond the 50-Ω environment in which the measurements for model identification were made. The PHD behavioral model faithfully represents driven nonlinear systems with mismatches at both the fundamental and harmonics. This enables the accurate simulation of distortion through cascaded chains of nonlinear components, thus providing key new design verification capabilities for RF and microwave modules and subsystems.

The new experiment design and model generation algorithms have been applied in the simulation environment starting from a circuit-level model of the IC. The improved experiment design and model identification procedure can also be applied to automated large-signal measurements using a VNNA.

The current experiment design dramatically reduces the number of measurements required to identify the model and reduces the size and complexity of the data. The methods result in a determination of the separate and independent contributions to the S and T model coefficients from specific orders of the mixing products, providing the optimal orthogonal excitation design and model generation processes. In the simulation-based application, the new excitation design rigorously insures that only the ideal linearized response to the large-signal tone is produced by the simulator, thus enabling a direct closed-form formula for the model identification of the S- and T-parameters. The simulation necessary to virtually excite the detailed circuit-level model for generating the behavioral model is based on the efficient SM analysis method. This method uses quantities already computed by the HB analysis of the system driven by a large input tone in order to evaluate the rigorously linear response of the system around this tone. It is much faster than a two-tone HB analysis.

This study, taken together with the companion experimental study in [5], has demonstrated a unified framework for automatically generating PHD amplifier behavioral models from both real VNNA measurements of a physical component and from a detailed circuit-level model of the component using the simulator. The PHD behavioral model faithfully represents driven nonlinear systems with mismatches at both the fundamental and harmonics. This enables robust, accurate, and useful simulation of distortion through cascaded chains of nonlinear components, thus providing key new design verification capabilities for RF and microwave modules and subsystems.

REFERENCES

[1] D. E. Root, J. Wood, and N. Tufillaro, "New techniques for nonlinear behavioral modeling of microwave/RF IC's from simulation and nonlinear microwave measurements," in *Proc. 40th ACM/IEEE Design Automation Conf.*, Anaheim, CA, Jun. 2003, pp. 85–90.

[2] J. Wood and D. E. Root, Eds., *Fundamentals of Nonlinear Behavioral Modeling for RF and Microwave Design*. Norwood, MA: Artech House, 2005.

[3] J. Wood, D. E. Root, and N. B. Tufillaro, "A behavioral modeling approach to nonlinear model-order reduction for RF/microwave ICs and systems," *IEEE Trans. Microw. Theory Tech.*, vol. 52, no. 9, pp. 2274–2284, Sep. 2004.

[4] J. C. Pedro, private communication, Jan. 2005.

[5] J. Verspecht, D. E. Root, J. Wood, and A. Cognata, "Broad-band multi-harmonic frequency domain behavioral models from automated large-signal vectorial network measurements," in *IEEE MTT-S Int. Microwave Symp. Dig.*, Long Beach, CA, Jun. 2005. [CD ROM].

[6] J. Verspecht, M. V. Bossche, and F. Verbeyst, "Characterizing components under large signal excitation: Defining sensible 'large signal S-parameters'," in *49th IEEE ARFTG Conf. Dig.*, Denver, CO, Jun. 1997, pp. 109–117.

[7] T. Van den Broeck and J. Verspecht, "Calibrated vectorial nonlinear-network analyzers," in *IEEE MTT-S Int. Microwave Symp. Dig.*, San Diego, CA, May 1994, pp. 1069–1072.

[8] P. Blockley, D. Gunyan, and J. B. Scott, "Mixer-based, vector-corrected, vector signal/network analyzer offering 300 kHz–20 GHz bandwidth and traceable phase response," in *IEEE MTT-S Int. Microwave Symp. Dig.*, Long Beach, CA, Jun. 2005. [CD ROM].

[9] E. Ngoya, N. Le Gallou, J. M. Nebus, H. Buret, and P. Reig, "Accurate RF and microwave system level modeling of wide band nonlinear circuits," in *IEEE MTT-S Int. Microwave Symp. Dig.*, Boston, MA, Jun. 2000, pp. 79–82.

[10] E. Ngoya and A. Soury, "Modeling memory effects in nonlinear subsystems by dynamic Volterra series," in *Proc. Int. Behavioral Modeling and Simulation Workshop*, San Jose, CA, Oct. 2003, pp. 28–33.

[11] J. Verspecht, "Method and test setup for measuring large-signal S-parameters," U.S. Patent Applicat. US 2004/0 257 092 A1, Dec. 23, 2004.

[12] A. Cidronali, K. C. Gupta, J. Jargon, K. A. Remley, D. DeGroot, and G. Manes, "Extraction of conversion matrices for p-HEMT's based on vectorial large-signal measurements," in *IEEE MTT-S Int. Microwave Symp. Dig.*, Philadelphia, PA, Jun. 2003, pp. 777–780.

[13] J. Verspecht, D. F. Williams, D. Schreurs, K. Remley, and M. D. McKinley, "Linearization of large-signal scattering functions," *IEEE Trans. Microw. Theory Tech.*, vol. 53, no. 4, pp. 1369–1376, Apr. 2005.

[14] "Agilent HMMC-5200 DC–20 GHz HBT series-shunt amplifier," Agilent Technol., Santa Rosa, CA, Data Sheet, Aug. 2002.

David E. Root (M'89–SM'01–F'02) received the B.S. degrees in physics and mathematics and Ph.D. degree in theoretical physics from the Massachusetts Institute of Technology (MIT), Cambridge, in 1986.

In 1985, he joined the Microwave Technology Center, Hewlett-Packard Company (now Agilent Technologies Inc.), Santa Rosa, CA. He originated and co-developed the commercial HP measurement-based large-signal HP field-effect transistor (HPFET) family of measurement-based transistor and diode models (Root models). Since 1997, he has twice managed the Computer Aided Engineering, Modeling, and Advanced Characterization Group Microwave Technology Center, where he led the establishment of capabilities including characterization and modeling with advanced pulsed bias, pulsed S-parameters, and large-signal vector network analyzer instruments for proprietary research and development. He managed and co-developed the Agilent HBT compact model for III–V HBTs. He is currently Principal Research Scientist with Technologies, Components, and Architecture Research and Development Laboratory, Agilent Technologies Inc., Santa Rosa. His current responsibilities include nonlinear behavioral and device modeling, large-signal simulation, and nonlinear measurements for new technical capabilities, and business opportunities.

Dr. Root is a member of the IEEE Microwave Theory and Techniques Society (IEEE MTT-S) Committee on CAD (MTT-1) and the Technical Program Committee of the IEEE MTT-S International Microwave Symposium (IMS). He is a reviewer for the IEEE TRANSACTIONS ON MICROWAVE THEORY AND TECHNIQUES.

Jan Verspecht (M'94–SM'05) was born in Merchtem, Belgium, on December 12, 1967. He received the Electrical Engineering and Ph.D. degrees from the Vrije Universiteit Brussel (VUB), Brussels, Belgium, in 1990 and 1995, respectively.

From 1990 to 1999, he was a Research Engineer with the Hewlett-Packard Company. From 1999 to 2002, he was a Technical Lead with Agilent Technologies Inc. In 2003, he became Director and Chief Consultant with Jan Verspecht bvba, Londerzeel, Belgium. He has authored over 30 conference papers, 11 refereed publications, and the ARFTG short course on "Large-Signal Network Analysis." His research interests include the large-signal characterization and behavioral modeling of RF, microwave, and digital components.

Dr. Verspecht is a member of the Automatic RF Techniques Group (ARFTG). He was the recipient of the 2002 ARFTG Technology Award.

David Sharrit received the B.S.E.E. degree from Arizona State University, Tempe, in 1970.

In 1973, he joined the Hewlett-Packard Company (now Agilent Technologies Inc.), Santa, Rosa, CA, where he was initially involved with 8505, 8568, and 8510 instruments prior to defining and managing the 8753 RF Vector Network Analyzer. He then managed the initial development of the Microwave Nonlinear Simulator (MNS) microwave nonlinear circuit simulator now used in the Agilent EEsof ADS and RFDE products. Returning to instruments, he managed the microwave transition analyzer (MTA) and invented the digital filtering algorithms used in recent spectrum analyzer digital IFs. Rejoining the computer-aided engineering (CAE) team, he then invented CE analysis, and was involved with additional simulator capabilities including behavioral modeling technologies. He holds several patents in the above areas.

Mr. Sharrit was the recipient of the 1992 ARFTG Technology Award.

John Wood (M'87–SM'03) received the B.Sc. and Ph.D. degrees in electrical and electronic engineering from The University of Leeds, Leeds, U.K., in 1976 and 1980, respectively.

From 1983 to 1997, he was a member of the academic staff of University of York, York, U.K., where he was responsible for teaching and research in solid-state electronics and microwave device and circuit technology. In 1997, he joined the Microwave Technology Center, Hewlett-Packard Company (now Agilent Technologies Inc.), Santa Rosa, CA, where his research has included the investigation and development of analytic large-signal field-effect transistor (FET) models and bias-dependent linear FET models for millimeter-wave applications, HBT modeling, and nonlinear behavioral modeling using large-signal network analyzer measurements and nonlinear system identification techniques. He is currently a Senior Technical Contributor responsible for RF computer-aided design (CAD) and modeling with the RF Division, Freescale Semiconductor, Tempe, AZ. He has authored or coauthored over 70 papers.

Alex Cognata received the Associate of Science degree in electronic technology from Santa Rosa Junior College, Santa Rosa, CA, in 1983.

He is currently with Agilent Technologies Inc., Santa Rosa, CA, where he develops measurement system hardware and software for nonlinear measurement systems. He co-developed a vector-corrected 45-MHz–50-GHz harmonic load–pull system with capabilities of measuring intermodulation distortion under tuned conditions. With this and other systems, he provides a wide variety of large signal measurement capabilities for model verification, FET and HBT device and process characterization, IC characterization, and stimulus response characterization for measurement-based behavioral modeling.